

# Low Power Consumption Micro C<sub>2</sub>H<sub>5</sub>OH Gas Sensor based on Micro-heater and Screen Printing Technique

*S. E. Moon<sup>1</sup>, H-K. Lee<sup>1</sup>, N-J. Choi<sup>1</sup>, J. Lee<sup>1</sup>, C. A. Choi<sup>1</sup>, W. S. Yang<sup>1</sup>, J. Kim<sup>1</sup>,  
J. J. Jong<sup>2</sup>, and D-J. Yoo<sup>2</sup>*

<sup>1</sup>ETRI, 138 Gajeong-ro, Yuseong-gu, Dejeon 305-700, Korea

<sup>2</sup>Sentech Korea, Sinchon-dong 21-6, Jimokro 75-gil, Paju-Si, Gyeonggi-Do, 413-170, Korea  
semoon@etri.re.kr

## Abstract

Micro C<sub>2</sub>H<sub>5</sub>OH gas sensor was fabricated based on micro-heater using tin oxide nano-powders with low power consumption and high sensitivity. Semiconducting SnO<sub>2</sub> nano-powders were synthesized via co-precipitation method, and to increase the sensitivity for alcohol gas rare metal dopants were added. In the structure of micro-heater, the resistances of two semi-circled Pt heaters are connected to the spreader for thermal uniformity. Based on the above design, low power consumption alcohol gas sensor was fabricated by using CMOS compatible MEMS process. Bridge type micro-heater based on Si substrate was fabricated by surface micromachining technique. Micro gas sensor showed substantial sensitivity down to 0.5 ppm alcohol at low power consumption (35 mW).

**Key words:** gas sensor, SnO<sub>2</sub>, micro-heater, surface micromachining, alcohol

## Introduction

Oxide semiconductors based gas sensors have been studied for several applications in detecting inflammable, toxic, and odorless gases. Moreover to reduce the power consumption of the device, the micro-heater to enhance the sensing and desorption of the target gas has been normally adopted [1-7].

In the group of hazardous gases, C<sub>2</sub>H<sub>5</sub>OH sensor is being focused to detect drunk driving or to detect leak in fuel cell. An extensive research is being carried out using various metal oxides like SnO<sub>2</sub>, ZnO, TiO<sub>2</sub>, WO<sub>3</sub>, In<sub>2</sub>O<sub>3</sub>, LaFeO<sub>3</sub> as sensor materials [8-15]. Due to the difficulties in MEMS design, fabrication technique and higher production cost for micro gas sensor, few commercial devices based on bulk micromachining technique are selling by pioneering company. This technology needs further improvement in handling device wafer and cost reduction for dry Si etching technique [16-24].

In this study we report surface micromachined gas sensors based on the SnO<sub>2</sub> thick film and micro-heater, which show low power consumption and high sensitivity for C<sub>2</sub>H<sub>5</sub>OH detection. The fabrication process for the micro gas sensor was based on the conventional complementary metal semiconductor (CMOS) compatible micro electro mechanical systems

(MEMS) processes for mass-production, which is possible to integrate with other devices and electronic circuitry.

## Experimental

Semiconducting SnO<sub>2</sub> nano-powders were synthesized by homogeneous co-precipitation method. NH<sub>4</sub>OH solution was slowly added to the aqueous solution of SnCl<sub>4</sub>·5H<sub>2</sub>O to control the pH value of the solutions, which is one of main parameters to determine the characteristics of nano-powders. And to suppress the growth of crystal in sintering process or to activate the reaction to the C<sub>2</sub>H<sub>5</sub>OH, other materials based on rare metals were added with constant stirring. The resulting gel was washed several times with the de-ionised water in order to remove the excess Cl<sup>-</sup> and NH<sub>4</sub><sup>+</sup> ions. The final milky white gel (precipitate) was then dried at 100 °C for 24 h. The obtained white powder was calcinated at 600 °C for 1 h.

The bulk X-ray diffraction (XRD) analysis of the powder was carried out for the Bragg angle (2θ) from 10 to 60° using Cu K<sub>α</sub> radiations. The average grain size of the powder was calculated using Scherrer formula

$$D = 0.9 \lambda / (\cos \beta)$$

where D is the average grain size, λ is the wavelength of the X-ray radiation used and β is

the angular width of the diffracted peak at the half maximum (FWHM) for the diffraction angle  $2\theta$ . In addition, further information about the particles size and shape was obtained by using scanning electron microscope (SEM). For SEM analysis, a thin conducting Pt layer (thickness 1–2 nm) was coated by using DC sputter.

To activate the gas sensing properties and to lessen the power consumption of the sensor, Si-based micro-heater was adapted, which was fabricated by using CMOS compatible MEMS processes. On these substrates SnO<sub>2</sub> nano-powders were deposited by screen printing technique.

Gas sensing properties were measured using a computer-controlled characterization system. The resistances of the sensor materials upon the Si micromachined micro-heater were measured. The response,  $R$ , is given by the rate of change in the resistance to the initial resistance,  $R = \Delta R/R_0 = |R_g - R_0|/R_0$ , where  $R_g$  and  $R_0$  are the resistance in the test gas and in air, respectively.

### Results and Discussion

Fig. 1 shows the XRD patterns of the doped SnO<sub>2</sub> nano-powders. All peaks belong to SnO<sub>2</sub> phase except one, which corresponds to Sn<sub>2</sub>O<sub>3</sub> phase. The calculated average grain size of the SnO<sub>2</sub> nano-powders using Scherrer formula was  $57 \pm 6$  nm, which grain size was proper to detect gas.

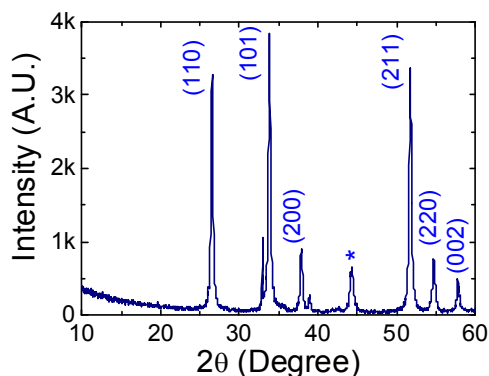


Fig. 1. XRD patterns of tin oxide nano-powders. \* corresponds to the Sn<sub>2</sub>O<sub>3</sub> phase.

Fig. 2 presents the SEM image and energy dispersive X-ray (EDAX) analysis result of the SnO<sub>2</sub> thick films on Si substrate. From the Fig. 2 (a), the distribution of the grain size of the SnO<sub>2</sub> nano-powders was uniform and nano-powders were mainly consisted of Sn and O element, as shown in Fig. 2 (b).

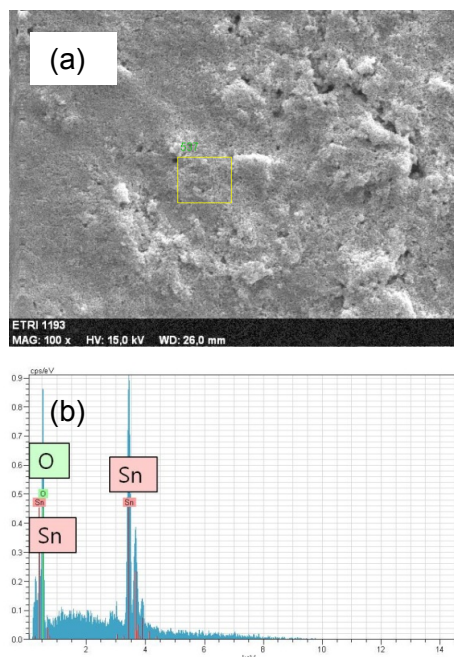


Fig.2. (a) SEM image and (b) EDAX analysis result of tin oxide nano-powders.

In the structure of the micro-heater, the resistances of two semi-circular Pt heaters are connected to the track for power supply. The resistance of each heating element becomes an electrically equal Wheatstone-bridge, which is divided in half by the heat-spreading structure. The generated heat diffuses from the circled heating elements through the heat spreaders to promote thermal uniformity at the central area where the sensing material will be located, which is thermally isolated by air using a bridge structure. The power consumption of the micro-heater device was simulated using the commercial finite element method (FEM) software (COMSOL). In the simulation, 400 °C temperature and the uniform thermal distribution at the center of the micro-heater were obtained in the expanse of 10 mW power consumption as shown in Fig. 3.

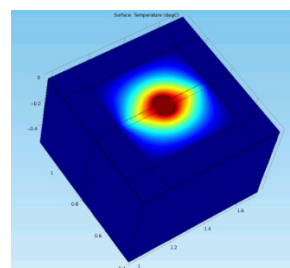


Fig. 3. Temperature distribution of micro-heater with 10 mW power consumption by using commercial finite element method simulation software

The low power consumption micro-heater was fabricated through a CMOS compatible MEMS processes, which was designed to endure high stress and to facilitate the fabrication processes. The detailed fabrication processes are shown in Fig. 4 with cross sectional schematic diagram and device picture after process. The thicknesses of the  $\text{SiO}_2$  and the  $\text{SiN}_x$  layer were determined to eliminate the residual tensile or compressive stress. The heating electrode and sensing electrode were patterned using a conventional lift-off process. The dry Si etching process with  $\text{XeF}_2$  gas after sensing material deposition was the last step in the micro gas sensor fabrication process. Because the Si dry etching process using the  $\text{XeF}_2$  gas did not damage the metal oxide thick film formed by the screen printing method, all the device fabrication processes were based on 6 inch Si substrate and were CMOS-compatible.

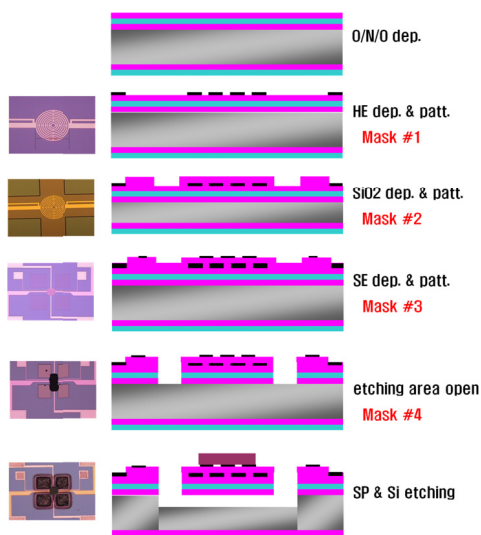


Fig. 4. Fabrication processes for  $\text{C}_2\text{H}_5\text{OH}$  gas sensor by using CMOS compatible MEMS process

To investigate the power consumption characteristics of the micro-heater, the temperature-dependent resistance of the micro-heater was measured using four-wire resistance measurement method. The measured temperature-dependent resistance values were compared with the values that can be calculated in the applied operation power to the micro-heater. Fig. 5 shows that the power consumption of the micro-heater was approximately linear characteristic to the operation temperature, and that a  $450\text{ }^\circ\text{C}$  temperature was attained at the expense of about 15 mW power consumption.

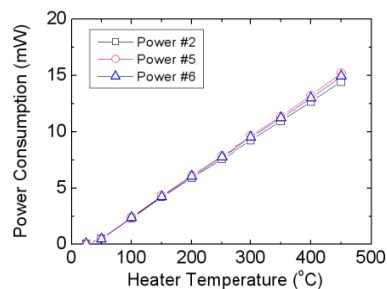


Fig. 5. Power consumption characteristics of surface micromachined micro-heater.

A photograph of the packaged micro gas sensor based on metal oxide thick film is shown in the Fig. 6. In the  $\text{C}_2\text{H}_5\text{OH}$  gas sensor in TO-5 can package, gold wires were wire-bonded between the Pt metal pad in the gas sensor and the pad in the TO-5 can for the necessary electrical connections. In the enlarged SEM image of the micro gas sensor, square shaped sensing  $\text{SnO}_2$  thick film exist in the center of O/N/O bridge in the square shaped surface micromachined Si etching area, where heating element exist inside, by using 4 opened square Si area.

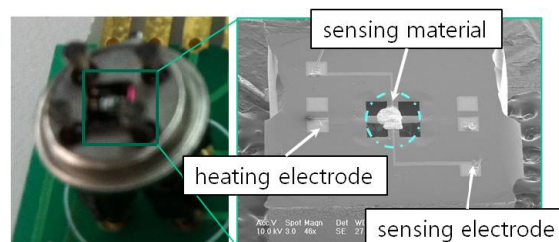


Fig. 6. Packaged  $\text{C}_2\text{H}_5\text{OH}$  gas sensor (left) and enlarged SEM image of the sensor.

As shown in Fig. 7,  $\text{SnO}_2$  nano-powders (generally n-type semiconductor) devices showed a conductance decrease at different concentrations of 0.5 to 2 ppm  $\text{C}_2\text{H}_5\text{OH}$  gas and the sensing response increased with an increasing  $\text{C}_2\text{H}_5\text{OH}$  concentration. The flow time of the target gas was 30 seconds, the response was nearly saturated for all the concentrations, and the initial resistance was recovered after the air gas was purged. The power consumption of the sensor was about 35 mW, which is much lower than that of the commercial semiconducting gas sensor [25]. The sensor device showed response (R) values of about 0.68 and 0.78 for 0.5 and 2 ppm  $\text{C}_2\text{H}_5\text{OH}$ , respectively. The measured power consumption of the micro gas sensor was much higher than that of the micro-heater, and it can be attributed to the thermal mass of the gas detection materials.

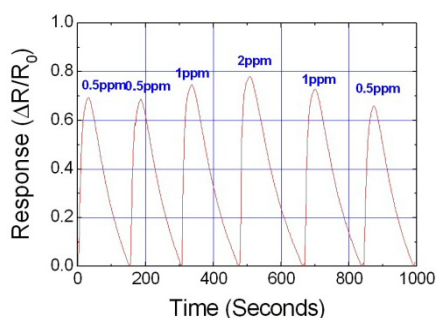


Fig. 7.  $C_2H_5OH$  gas sensing properties of the fabricated micro gas sensor with 35 mW power consumption

### Summary

Micro  $C_2H_5OH$  gas sensor was fabricated based on micro-heater using tin oxide nanoparticles with low power consumption and high sensitivity. The device was fabricated by using CMOS compatible MEMS process and the sensing material was deposited by using screen printing technique. Micro gas sensor showed substantial sensitivity down to 0.5 ppm alcohol at low power consumption (35 mW).

### Acknowledgements

This work was supported by Technology Innovation Program (Innovation Cluster Program) through the Korea Innovation Cluster Foundation funded by the Ministry of Knowledge Economy (MKE, Korea) and by the IT R&D program of the MKE/KEIT [10035570, Development of self-powered smart sensor node platform for smart&green building].

### References

[1] Y-J. Chen, X. Y. Xue, Y. G. Wang, and T. H. Wang, *Appl. Phys. Lett.* 87, 233503-1-3 (2005).  
 [2] S. J. Tans, A. R. M. Verschueren, and C. Dekker, *Nature* 393, 49-52 (1998).  
 [3] X. Duan, Y. Huang, Y. Cui, J. Wang, and C. M. Lieber, *Nature* 409, 66-69 (2001).  
 [4] J. Hahm and C. M. Lieber, *Nano Letters* 4, 51-54 (2004).  
 [5] C. Li, D. Zhang, X. Liu, S. Han, T. Tang, J. Han, and C. Zhou, *Appl. Phys. Lett.* 82, 1613-1615 (2003).  
 [6] J. Li, Y. Lu, Q. Ye, M. Cinke, J. Han, and M. Meyyappan, *Nano Letters* 3, 929-934 (2003).  
 [7] J. Kong, N. R. Franklin, C. Zhou, M. G. Chapline, S. Peng, K. Cho, and H. Dai, *Science* 287, 622-625 (2000).

[8] J. C. Belmonte, J. Manzano, J. Arbiol, A. Cirera, J. Puigcorbe, A. Vila, N. Sabate, I. Gracia, C. Cane, and J. R. Morante, *Sensors and Actuators B* 114, 881-892 (2006).  
 [9] M. Graf, D. Barrentino, K-U. Kirstein, and A. Hierlemann, *Sensors and Actuators B* 117, 346-352 (2006).  
 [10] T. Iwaki, J. A. Covington, F. Udrea, S. Z. Ali, P. K. Guha, and J. W. Gardner, *Journal of Physics C* 15, 27-32 (2005).  
 [11] S. E. Moon, J-W. Lee, S-J. Park, J. Park, K-H. Park, and J. Kim, *J. Korean Phys. Soc.* 56, 434-438 (2010).  
 [12] A. D. DeHennis and K. D. Wise, *Journal of Microelectromechanical Systems* 14, 12-18 (2005).  
 [13] C. Hagleitner, A. Hierlemann, D. Lange, A. Kummer, N. Kerness, O. Brand and H. Baltes, *Nature* 414, 293-296 (2001).  
 [14] I-S. Hwang and J-H. Lee, *J. Nanoeng. Nanomanuf.* 1, 1-7 (2011).  
 [15] S. J. Park, J. Park, H-Y. Lee, S. E. Moon, K-H. Park, J. Kim, S. Maeng, F. Udrea, W. I. Milne, and G. T. Kim, *Journal of Nanoscience and Nanotechnology* 10, 3385-3388 (2010).  
 [16] L. Zhao, M-S. Choi, H-S. Kim, and S-H. Hong, *Nanotechnology* 18, 445501-1-5 (2007).  
 [17] S. E. Moon, H-Y. Lee, J. Park, J-W. Lee, N-J. Choi, S-J. Park, J-H. Kwak, K-H. Park, J. Kim, G-H. Cho, T-H. Lee, S. Maeng, F. Udrea, and W. I. Milne, *Journal of Nanoscience and Nanotechnology* 10, 3189-3192 (2010).  
 [18] F. H. Ramirez, A. Tarancon, O. Casals, J. Arbiol, A. R. Rodriguez, and J. R. Morante, *Sensors and Actuator B* 121, 3-17 (2007).  
 [19] M. C. Carotta, S. Gherardi, C. Malagu, M. Nagliati, B. Vendemiati, G. Martinelli, M. Sacerdoti, and I. G. Lesci, *Thin Solid Films* 515, 8339-8344 (2007).  
 [20] V. N. Singh, B. R. Mehta, R. K. Joshi, and F. E. Krus, *Journal of Nanoscience and Nanotechnology* 7, 1930-1933 (2007).  
 [21] K. Ryu, D. Zhang, and C. Zhou, *Appl. Phys. Lett.*, 92, 093111-1-3 (2008).  
 [22] G. Zhang and M. Liu, *Sensors and Actuator B* 69, 144-152 (2000).  
 [23] N. S. Ramgir, I. S. Mulla, and K. P. Vijayamohan, *Sensors and Actuator B* 107, 708-715 (2005).  
 [24] E. Comini, G. Faglia, G. Sberveglieri, D. Calestani, L. Zanotti, and M. Zha, *Sensors and Actuator B* 111-112, 2-6 (2005).  
 [25] [www.figaro.co.jp](http://www.figaro.co.jp).